Proceedings World Geothermal Congress 2026
Calgary, Canada, June 8 – 11, 2026

Optimization of Vacuum Insulated Tubulars for Geothermal U-Shaped Wellbores: Modeling Challenges and Performance Enhancement Under Supercritical CO2 Conditions

Nasikul Islam[1], Corey Dufrene[2] and Elizabeth Cambre[2]

Exceed Geo Energy[1], Valloruec[2]

Keywords: U-Tube, Closed Loop Geothermal, Advanced Geothermal System, Supercritical CO2, Wellbore modeling, Vacuum Insulated Tubular, Next Generation Geothermal, Natural Convection

ABSTRACT

Vacuum Insulated Tubulars (VITs) offer a highly effective pathway for increasing thermal efficiency and power output in closed loop geothermal systems (CLGS) by substantially reducing heat loss as the working fluid travels from the reservoir to the surface, thereby preserving high temperature energy that would otherwise dissipate into the surrounding formation. This retained thermal energy directly enhances surface production temperature, improves thermodynamic efficiency, and increases net electrical power generation. This study evaluates the optimization of a large diameter VIT string installed in the production leg of a U-shaped geothermal well in Presidio County, Texas, where the reservoir behaves like a sedimentary wet rock system and natural convective flow within porous, fractured formations enhances heat extraction. The analysis examines key design parameters such as VIT length, mass flow rate, and thermal performance under supercritical CO_2 (sCO_2) conditions. Results show that deploying 50% VIT coverage (13 3/8inch outer diameter with a 9 5/8inch inner diameter) at a flow rate of 250 kg/s and a bottomhole temperature of 217.7 °C increases power output by approximately 1.35 MWe relative to the 10.18 MWe baseline without VIT, using a representative industry thermal-to-electric efficiency of 23%. This VIT configuration yields a projected return-on-investment (ROI) in 1.53 years.

1 INTRODUCTION

Closed-loop geothermal systems (CLGS) extract heat by circulating a working fluid, typically water or sCO_2, through sealed wellbore tubing, enabling energy production without relying on natural fractures or reservoir permeability. Because the fluid remains isolated from the formation, CLGS avoid scaling, corrosion, and mineral deposition common in open-loop hydrothermal or Enhanced geothermal systems (EGS) operations and offer a controllable thermal-hydraulic environment for power generation (White et al., 2024). CLG wells are commonly implemented in either coaxial or U-tube configurations. Coaxial designs use a concentric pipe arrangement, often incorporating vacuum-insulated tubing (VIT) on the production path to reduce thermal losses, whereas U-tube designs employ two parallel strings connected at depth to form a balanced circulation loop capable of higher mass-flow operation (White et al., 2024).

Incorporating convective heat flow into U-tube CLGS systems underscores the importance of selecting a reservoir with suitable permeability. Simulations of U-tube CLGS in water-saturated rock show that once reservoir permeability reaches the hundreds of millidarcies, around 250 mD, natural convection begins to significantly boost heat transport to the wellbore. As a result, the system delivers meaningfully higher thermal output compared with conduction-only reservoirs (White et al., 2024).

The choice of working fluid is another major lever for increasing power output in CLGS. As a subsurface working fluid, sCO_2 provides high density, low viscosity, and favorable heat-transfer characteristics that enable efficient heat uptake along the U-tube. These thermophysical properties also translate directly into advantages for surface power conversion. When expanded through a Brayton-cycle turbine, sCO_2 supports compact, high-efficiency turbomachinery with significantly smaller footprints than steam-based systems. The U.S. Department of Energy notes that sCO_2 power cycles can achieve higher thermal efficiencies than state-of-the-art steam Rankine cycles and offer >50% efficiency potential under high-temperature heat sources (U.S. DOE, 2024).

Demonstrating this, the 10-MWe Supercritical Transformational Electric Power (STEP) pilot plant has already completed Phase 1 testing, achieving full turbine operation at 500 °C and 250 bar and generating 4 MWe of grid-synchronized power (Power Magazine, 2024). Phase 2 will reconfigure the plant with a turbine inlet temperature of 715 °C, where DOE aims to validate thermal efficiencies exceeding 50% (NETL, 2024).

However, CLGS under investigation in this paper operate at substantially lower production temperatures (~220 °C). Accordingly, this study adopts the 23% thermal-to-electric conversion efficiency used by White et al., who modeled a sCO_2 expansion cycle at ~190 °C with a fixed turbine outlet pressure of 8.1 MPa for U-tube CLGS designs. This value reflects realistic thermodynamic limits for present geothermal operating conditions rather than the upper bound achievable by high-temperature sCO_2 Brayton cycles.

1.1 Geothermal Potential in Presidio County, Texas

Presidio County lies within the Trans-Pecos region of West Texas, an area characterized by elevated geothermal gradients and deep sedimentary basins. Its geological setting, combined with low population density and access to existing transmission corridors, positions the county as a strong candidate for CLG development.

According to the *Presidio County Geothermal Assessment* conducted by the Bureau of Economic Geology (BEG) at the University of Texas at Austin (Wisian et al., 2024), the county contains "substantial, undeveloped geothermal resources" with the potential to supply many times its present electrical and direct-use demand. The assessment identifies the county's highest-quality geothermal zone, the Border Region, as a ~16 km (10 mi) wide corridor along the Rio Grande extending from Redford toward the northwest corner of the county. This region exhibits exceptionally high geothermal gradients of approximately 50 °C/km, allowing shallower drilling depths and improving overall project economics (Wisian et al., 2024). Recent offset-well temperature data compiled from Enverus and USGS indicate temperatures of approximately 127 °C at 8,196 ft; when extrapolated to planned drilling depths of ~15,000 ft, these data suggest bottom-hole temperatures on the order of ~213 °C within the deeper Paleozoic interval, including the Cambrian basement.

The BEG assessment further notes that much of the interior two-thirds of Presidio County also maintains above-average geothermal temperatures relative to global continental norms. Although these interior areas are cooler than the Border Region, they still possess economically viable potential for both power generation and direct-use applications (Wisian et al., 2024). In addition to favorable thermal conditions, Presidio County benefits from its proximity to extensive oil- and gas-sector activity across West Texas. This mature industrial ecosystem provides access to drilling expertise, well-construction infrastructure, and experienced service providers, factors that can reduce development costs and accelerate geothermal project timelines (Tison, 2024).

Structurally, Presidio County lies within the tectonically active Trans-Pecos province, where Basin-and-Range–style extension and proximity to the Rio Grande rift have produced a naturally fractured crust. Although the BEG (Wisian et al., 2024) does not quantify fracture permeability directly, it reports high geothermal gradients and shallow Precambrian basement in the Border Region. A multiscale subsurface assessment by Bhattacharya et al. (2025) similarly describes the Border Region as lying within a structurally complex zone influenced by the Rio Grande rift.

Given these elevated gradients and structurally energized conditions, a U-tube CLGS is well-positioned to capture heat efficiently in this setting.

1.2 Harnessing Geothermal Energy with U-Tube CLGS

U-tube CLGS configurations are emerging as a leading design for high-capacity geothermal power generation because their hydraulic performance is fully engineered and independent of reservoir permeability. Unlike conventional EGS wells, where circulation rates are constrained by fracture transmissivity and reservoir injectivity, CLGS circulate fluid entirely within the wellbore. The U.S. Department of Energy notes that CLGS "are not dependent on the permeability or water accessibility of conventional geothermal," emphasizing that flow is controlled by tubing hydraulics rather than formation permeability (DOE, 2024). Numerical CLGS studies from the Closed-Loop Geothermal Working Group further confirm that U-tube and coaxial designs treat mass-flow rate as an engineering variable, determined by tubing diameter, frictional resistance, and pump capacity, rather than a geologic constraint (Beckers et al., 2023). As a result, U-tube systems can be engineered to sustain substantially higher circulation rates than EGS wells.

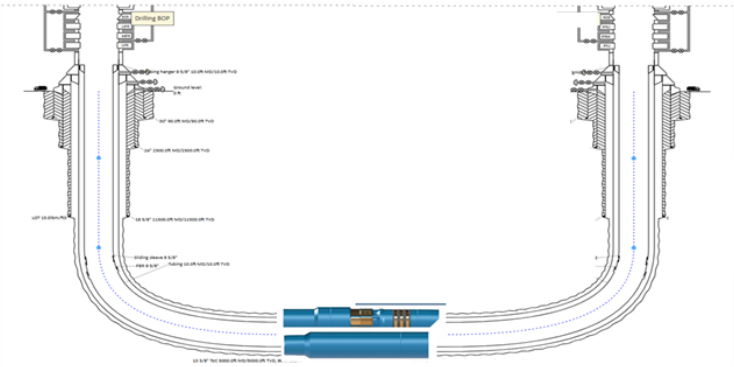
In U-tube CLGS, VIT is required only in the production leg because this section carries the heated fluid upward after absorbing thermal energy from the reservoir. As the fluid ascends, the temperature differential between the hot production stream and the cooler surrounding formations increases significantly, creating the highest potential for thermal losses. Without insulation, the produced fluid would lose heat to the formation, reducing overall thermal efficiency and lowering the temperature ultimately delivered at surface.

In contrast, the injection leg does not benefit from VIT because the descending fluid is comparatively cold and is continuously gaining heat from the surrounding rock. Applying insulation would restrict this heat uptake and provide no technical or economic advantage.

Because VIT is one of the most cost-intensive components in CLG well construction, the study evaluates a range of VIT lengths to identify the minimum insulated interval needed to maintain high production-leg temperatures while avoiding unnecessary material expenditure. Although the working fluid does continue to gain heat in the lower section of the production leg, particularly near the lateral where formation temperatures are highest, the dominant thermal challenge occurs higher in the wellbore. As the fluid ascends, the temperature differential between the hot production stream and the cooler upper formation increases sharply, leading to significant potential for heat loss if insulation is insufficient.

In Figure 1, the CLGS consists of two twin wells connected at the midpoint of the lateral through an intentional wellbore interception. The connection is accomplished using standard well construction components, including a metal-to-metal seal, a polished bore receptacle, and a casing packer.

Figure 1. U-Tube CLG Well Configuration.



1.3 Cementing and Thermal Conductivity Considerations

In a U-tube CLGS, the cement sheath acts as a key thermal interface between the formation and the circulating fluid. Maximizing heat uptake begins in the injection leg, where the fluid enters the well at its coolest and has the largest temperature difference with the surrounding rock. Thermally conductive cements are most effective in this interval because they promote efficient heat transfer into the tubing. Laboratory studies show that dense cements achieve thermal conductivities in the ~0.8–1.5 W/m·K range due to their continuous solid conduction networks (Abid et al., 2024; Wang et al., 2020). In contrast, foamed cements contain higher gas fractions and disrupted conduction pathways, yielding much lower thermal conductivities, typically ~0.30–0.40 W/m·K, (Zhou et al., 2023; Zhang & Li, 2022).

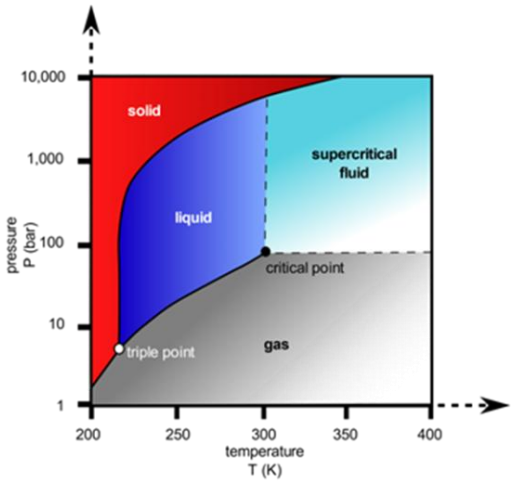
The horizontal lateral should remain uncemented, as any cement layer would act as an unnecessary thermal barrier. An open lateral allows direct conductive and convective contact between the rock and the outer wall of the U-tube, maximizing the lateral's contribution to overall heat extraction.

Along the production leg where formation temperatures decline toward surface, particularly in wells without VIT, an insulative cement becomes advantageous by limiting heat loss to cooler upper formations. Published geothermal wellbore studies show that both conductive and insulative cements have roles depending on depth-dependent temperature differences, making cement placement a function of the local thermal gradient rather than a single design applied uniformly along the production interval (Abid et al., 2024; Zhou et al., 2023; Zhang & Li, 2022).

1.4 Advantages of sCO_2 as a Geothermal Working Fluid

Understanding the phase behavior of CO_2 is essential for evaluating its performance as a working fluid in geothermal heat extraction and power generation. The CO_2 phase diagram, as depicted in Figure 2, provides the framework for determining how temperature and pressure conditions govern the transition into the supercritical state.

Figure 2. CO2 Phase Diagram (FavPNG, n.d.)



SCO_2 enters the injector well at a surface pressure of approximately 2,000 psi (137.9 bar), where it begins its descent through the wellbore. As the fluid moves through the CLGS, increasing temperature and pressure push the CO_2 fully into its supercritical state. The CO_2 phase diagram defines how temperature and pressure conditions control the transition into the supercritical state, including the critical point at approximately 304.15 K (31°C) and 73 bar.

A key driver of circulation in this configuration is the thermosiphon effect, in which density differences between cooler descending CO_2 and hotter ascending CO_2 create a natural buoyancy force. This effect reduces or eliminates the need for surface pumping and enables continuous, energy-efficient circulation through the U-tube system (Nielson et al. 2022).

SCO_2 also delivers superior thermal performance compared to water-based working fluids. Its low viscosity reduces frictional pressure losses along the 1,200-ft lateral and vertical wellbores, allowing it to flow with minimal resistance and maintain higher mass flow rates. An additional factor influencing CO_2 behavior in the wellbore is the Joule–Thomson (JT) effect, which describes the temperature change a fluid undergoes during pressure drop at constant enthalpy.

Third Party Commercial Software for Thermal and Flow Simulation

To support the thermal modeling and system optimization, this study utilizes a third-party software, a specialized simulation tool for geothermal well design. The software enables detailed modeling of convection and conductive heat transfer, fluid flow, and insulation performance. It supports multi-phase flow analysis and can simulate the behavior of sCO_2 under varying pressure and temperature conditions. Using the software, the study will simulate the thermal profile of the U-tube system, evaluate the effectiveness of VIT, and determine the optimal configuration for maximizing energy recovery.

2 METHODOLOGY

This section outlines the technical approach used to evaluate the performance of a U-tube CLGS utilizing sCO_2 as the working fluid. The methodology includes the wellbore configuration, casing and cement design, reservoir characterization, thermodynamic inputs, and simulation workflows.

2.1 Wellbore Configuration

The geothermal well is designed with a U-tube CLG configuration, consisting of vertical sections of 16,000 feet and a lateral section of 1,200 feet. The working fluid circulates down one leg of the U-tube and returns through the other, absorbing heat from the surrounding formation. The tubing size is 13 3/8 inches, with VIT modeled as 9 5/8 inches nested within the larger casing. The VIT is deployed in the production leg to minimize thermal losses and preserve fluid temperature during return flow.

2.2 Casing and Cementing Design

The wellbore is planned with a 22-inch diameter to provide sufficient clearance for the casing and insulation system. The primary structural casing consists of 18 5/8-inch OD steel, inside which a 13 3/8-inch casing is run along the full vertical and lateral length. In the production leg, a 9 5/8 × 13 3/8-inch VIT string is installed.

The vertical section of the well extends to 16,000 ft and is fully cemented for zonal isolation and structural integrity. For this analysis, a thermally conductive cement with a conductivity of 1.5 W/m·K was applied along the entire vertical interval, including the production leg. Because the upper portion of the production leg is insulated with VIT, the presence of higher-conductivity cement in that interval does not influence the results. The vacuum insulation governs heat transfer in that section, effectively isolating it from cement-related effects.

In contrast, the 1,200-ft horizontal lateral remains uncemented to maximize direct thermal contact between the casing and the formation within the primary heat-exchange zone.

Material properties incorporated into the model include a thermal conductivity of 43 W/m·K for steel casing and 0.04 W/m·K for the VIT, reflecting its high-performance insulation characteristics. These parameters were used to simulate heat-transfer behavior and to evaluate the influence of VIT length on overall energy recovery efficiency.

In the 1,200-ft horizontal lateral, the model employs the borehole option, which treats the interval as an open annulus in direct thermal communication with the surrounding formation rather than as a cemented or cased section. This approach allows the simulator to capture natural reservoir convection, enabling in-situ formation fluids to circulate and transfer heat to the wellbore more effectively. By using the borehole representation, the model accounts for both conductive and convective heat transport mechanisms within the lateral, which is essential because this section represents the primary heat-exchange zone where formation temperatures are highest, and heat uptake is most active.

Table 1 outlines the wellbore design for the scenario with 50 % VIT in the production leg.

	Top (ft)	Bottom (ft)	ID (in)	OD (in)	Rugosity (μm)	Thermal Conductivity (W/m*K)	Type
Inject. Leg	17,200	33,200	18.625	22.000	0.0	3.5	Cement
Inject. Leg	17,200	33,200	17.025	18.625	0.0	43	Casing
Inject. Leg	17,200	33,200	12.250	13.375	0.0	43	Tubing
Lateral	16,000	17,200	13.375	N/A	0.0	N/A	Borehole
Lateral	16,000	17,200	12.250	13.375	0.6	43	Casing
Prod. Leg	0	16,000	18.625	20.000	0.0	1.5	Cement
Prod. Leg	0	16,000	17.025	18.625	0.6	43	Casing
Prod. Leg	0	8,000	8.535	9.625	0.0	43	Tubing
Prod. Leg	8,000	16,000	9.406	13.375	0.6	0.04	VIT

Table 1. U-Tube Wellbore Configuration Inputs in Commercial Software

2.3 Scenario Design

To assess the influence of insulation and fluid selection on system performance, the following scenarios were analyzed:

Category	Scenario	Details
Insulation Variations (VIT Deployment)	No VIT (Baseline)	9 5/8-inch tubing
	50% VIT Coverage	8,000 ft of VIT on production leg
	100% VIT Coverage	16,000 ft of VIT on production leg
Working Fluid Comparison	Supercritical CO_2	High-efficiency cycle
	Water	Conventional geothermal fluid
VIT Size Modeled	Inner Pipe	9 5/8-inch diameter
	Outer Pipe	13 3/8-inch diameter
Analysis Basis	All Scenarios	Production inside 9 5/8-inch casing
Hole Size	Production Hole	16-inch diameter

Table 2: Modeling Assumptions for VIT Deployment and Working Fluid

Each scenario was evaluated for its impact on surface temperature and power output at the surface. The results were compared to determine the optimal configuration for maximizing energy recovery with lowest ROI.

2.4 Reservoir Properties

The formation properties used in the thermal modeling are as follows:

- Density: 2600 kg/m^3
- Specific Heat Capacity: 1.0 kJ/(kg·K)
- Thermal Conductivity: 3.5 W/(m·K)

2.5 Modeling Inputs for SCO_2

Thermodynamic properties of sCO_2 are central to the system's performance. Enthalpy inputs are derived from CO_2 property tables and equations of state, accounting for pressure, temperature, and phase behavior. The simulations incorporate CO_2's specific heat, density, and viscosity under supercritical conditions, enabling accurate modeling of heat absorption and fluid dynamics. The reservoir model for the Presidio County geothermal system was configured using depth-dependent pressure, temperature, and enthalpy values to represent realistic subsurface conditions. These key parameters are included in Table 3.

Category	Parameter	Value	Notes
Formation Pressure Profile	Pressure @ surface (0 ft)	~145 psi	
	Pressure @ 16,000 ft	~5801 psi	
	Pressure @ 17,200 ft (lateral)	~5801 psi	Lateral assumed isobaric
	Pressure @ 33,200 ft	~145 psi	Return to surface
Formation Temperature Profile	Temperature @ surface	25 °C	
	Temperature @ 16,000 ft	217.7 °C	
	Temperature @ lateral depth	217.7 °C	Same as vertical depth
Enthalpy	Enthalpy @ surface	~105.8 kJ/kg	
	Enthalpy @ depth	~946.8 kJ/kg	
Fluid Composition	CO_2 fraction	1.000	Pure CO_2
	H_2O fraction	0.000	
	NaCl fraction	0.000	
Specific Heat Capacity	Cp	2.0 J/kg·K	
Initial Conditions	Initial pressure	2000 psi	
	Initial enthalpy	−236.3 kJ/kg	
	Mass flow rate	540 t/h	Equivalent to 150 kg/s

Table 3. Modeling Inputs for Formation and SCO_2

2.6 Power Output Efficiency

The performance of sCO_2 is evaluated against water across all VIT configurations considered in this study. For the water-based cases, a conversion efficiency of 10% was applied, consistent with typical values for Organic Rankine Cycle (ORC). In contrast, sCO_2 scenarios use a higher conversion efficiency of 23%.

3 RESULTS

3.1 Surface Temperature for Different VIT Lengths Across Various Flow Rates

Figures 3, 4, and 5 present the modeled return surface temperature for sCO_2 under three insulation scenarios in a U-tube configuration: (1) no VIT with a 9 5/8-inch casing, (2) 50% VIT coverage, and (3) 100% VIT coverage along the production leg. Each plot displays the produced fluid temperature as a function of depth, allowing the effect of insulation length on the temperature profile to be visually compared.

Flow rates of 50, 100, 150, 200, and 250 kg/s were modeled for all three cases. In each scenario, the plots show how surface temperature varies with mass flow rate, with the highest return temperatures occurring at

intermediate flow rates, specifically 100 and 150 kg/s. As VIT coverage increases from 0% to 50% and then to 100%, the figures show progressively higher temperatures at the surface.

Figure 3. Fluid Temperature as a Function of Depth - 9 5/8-inch casing with no VIT with sCO_2

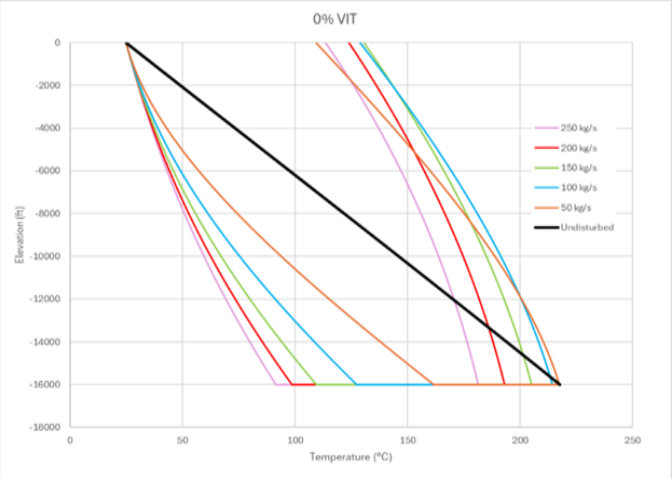


Figure 4. Fluid Temperature as a Function of Depth - 50 % VIT with sCO_2

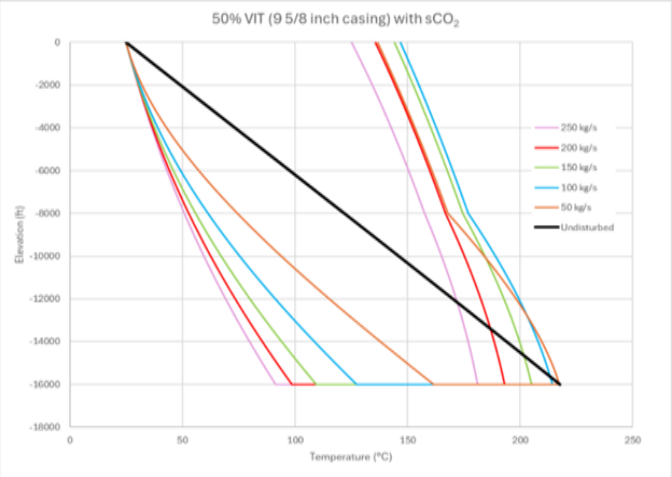
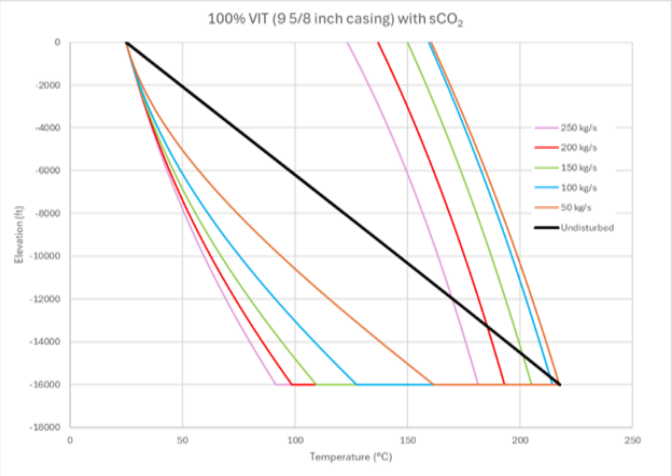


Figure 5. Fluid Temperature as a Function of Depth - 100 % VIT with sCO_2



Figures 6 through 9 present the modeled produced-temperature profiles for sCO_2 at flow rates of 100, 150, 200, and 250 kg/s under three insulation scenarios: no VIT, 50% VIT coverage, and 100% VIT coverage along the

production leg. The black line in all plots represents the undisturbed reservoir temperature gradient, providing a reference for the maximum temperature available within the formation.

Figure 6. Fluid Temperature as a Function of Depth - 100 kg/s of sCO2

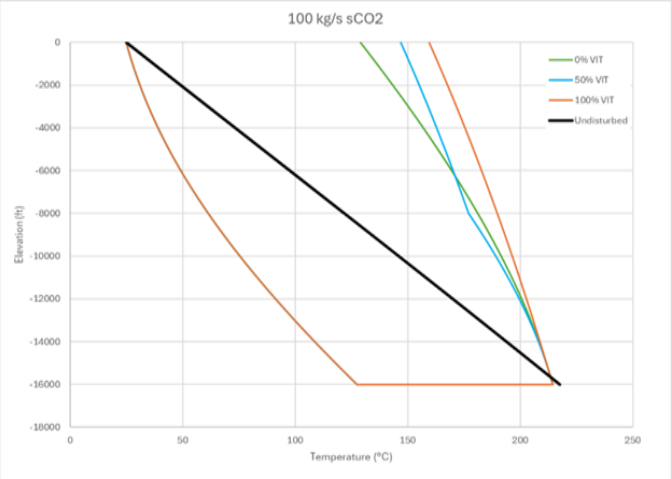


Figure 7. Fluid Temperature as a Function of Depth - 150 kg/s of sCO2

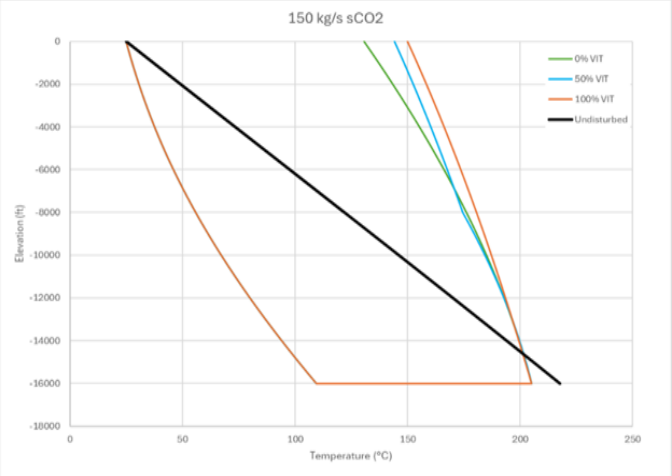


Figure 8. Fluid Temperature as a Function of Depth - 200 kg/s of sCO2

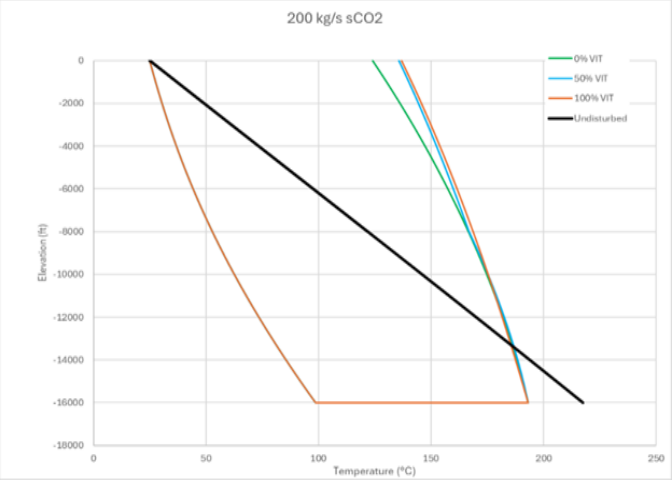
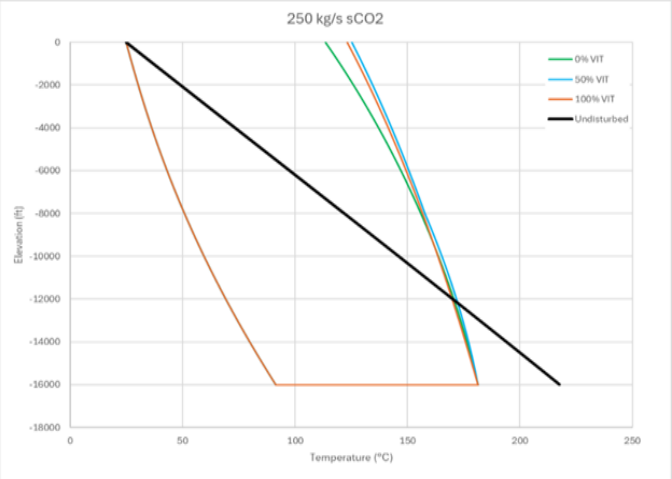


Figure 9. Fluid Temperature as a Function of Depth - 250 kg/s of sCO2



3.2 Electrical Power Output of Various VIT Configurations with sCO2 and Water

Figure 10 shows the electrical power output for the case with 0% VIT, illustrating how water and sCO_2 perform without insulation on the production leg. Figure 11 presents the results for 50% VIT coverage, showing the effect of partial insulation on the power curves for both fluids. Figure 12 displays the electrical output under 100% VIT coverage

Figure 10. Electrical Power Output of H2O and sCO_2 with 0% VIT at Various Flow Rates

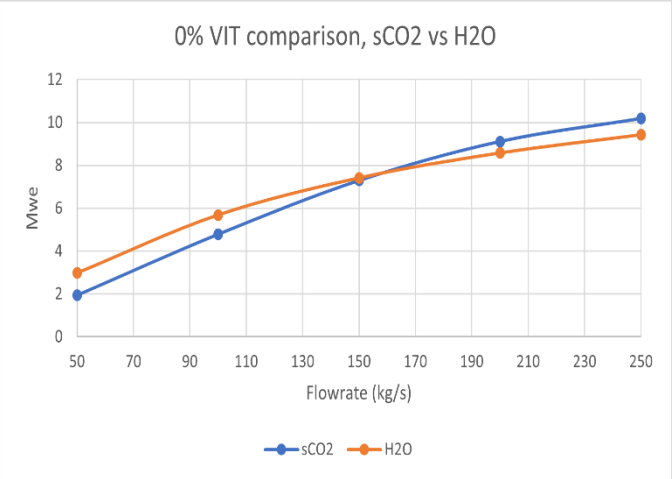


Figure 11. Electrical Power Output of H2O and sCO_2 with 50% VIT at Various Flow Rates

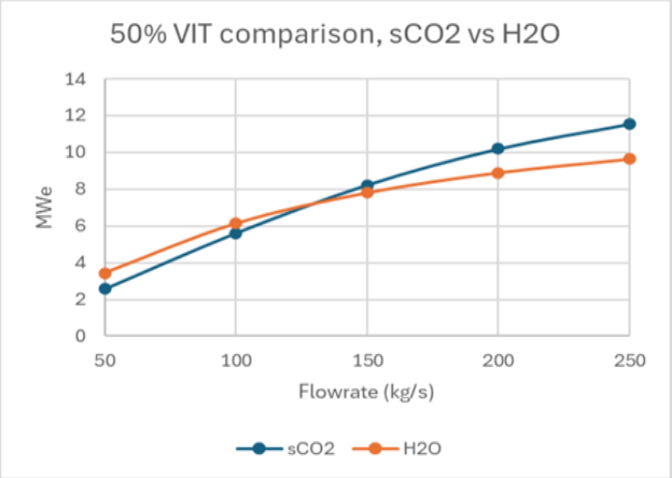


Figure 12. Electrical Power Output of H2O and sCO_2 with 100% VIT at Various Flow Rates

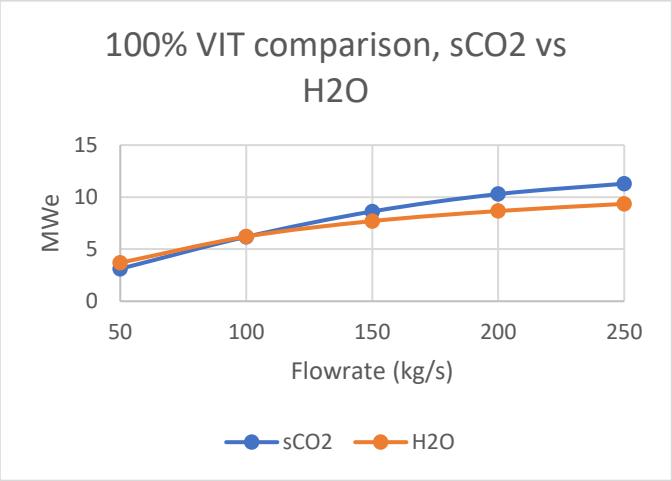


Figure 13 illustrates the electrical power output for sCO_2 for 0%, 50%, and 100% VIT coverage. Figure 14 shows the corresponding water results, allowing a direct comparison of how insulation influences electrical performance for the water-based system.

Figure 13. Electrical Power Output vs. Flowrate of sCO2 for 0,50,100 % VIT

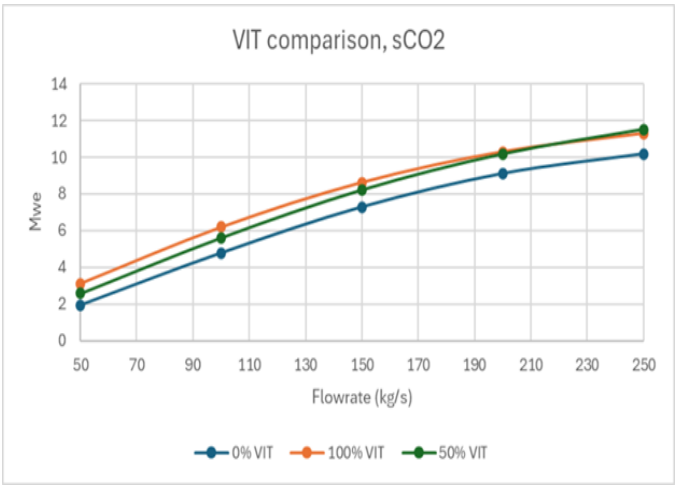
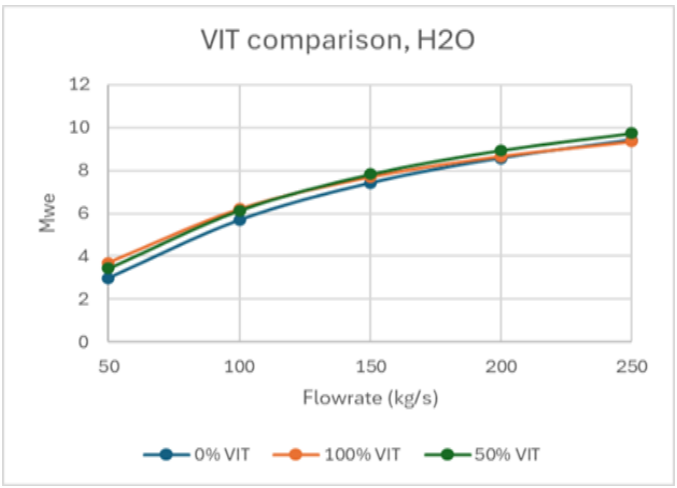


Figure 14. Electrical Power Output vs. Flowrate of H20 for 0,50,100 % VIT



3.3 Surface Temperature Behavior of Water vs. sCO_2 with 50% VIT

Figures 15 and 16 compare the modeled surface temperatures for water and sCO_2 at 150 kg/s and 250 kg/s under 50% VIT. These two flow rates are shown to highlight the transition point where the hotter produced fluid shifts from water at lower flow to sCO_2 at higher flow.

Figure 15. Surface Temperature Comparison for 50% VIT Using Water and sCO_2 at 250 kg/s

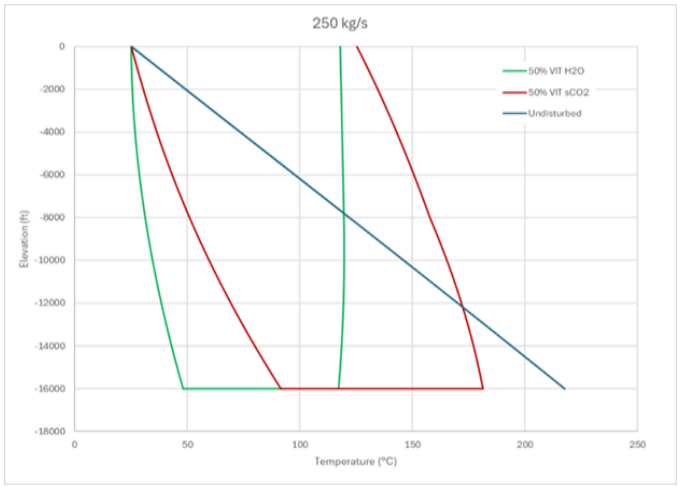
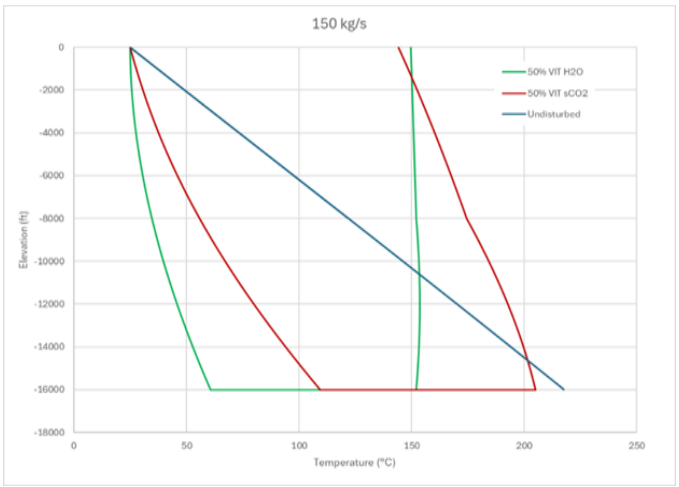


Figure 16. Surface Temperature Comparison for 50% VIT Using Water and sCO_2 at 150 kg/s



Figures 17 and 18 present the modeled thermal and electrical power output for water and sCO_2 circulating through a U-tube CLGS with 50% VIT insulation.

Figure 17. Thermal Power Output of Water vs. sCO_2 with 50% VIT Insulation

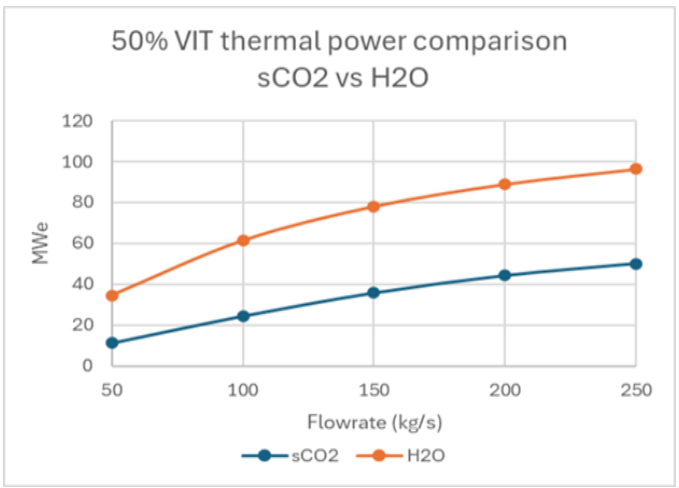


Figure 18. Electrical Power Output of Water vs. sCO_2 with 50% VIT Insulation

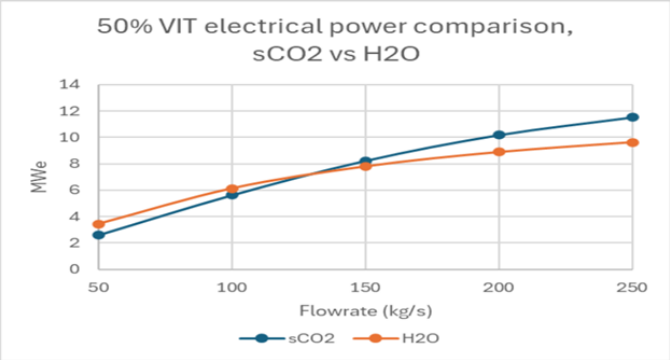


Table 4 summarizes the electrical power output and corresponding return-on-investment (ROI) in years for two insulation scenarios, 50% VIT and 100% VIT, across flow rates of 50, 100, 150, 200, and 250 kg/s. For each flow rate, the table lists the modeled electrical power generation and the associated ROI based on the assumed cost and performance parameters.

Table 4. Electrical Power Output and ROI in Years for 50 %, 100 % VIT at 50,100,150,200, and 250 kg/s

	kg/s	MWe	ROI (yrs)
50% VIT	50	2.57	3.3
	100	5.61	2.5
	150	8.23	2.2
	200	10.19	1.9
	250	11.53	1.5
100% VIT	**kg/s**	**MWe**	**ROI (yrs)**
	50	3.12	3.5
	100	6.19	2.9
	150	8.63	3.1
	200	10.29	3.5
	250	11.29	3.7

4 DISCUSSION

4.1 Surface Temperature and VIT Coverage

The results in Figures 3–9 show that VIT coverage has a strong effect on the surface temperature profile in a U-tube sCO_2 CLG well. The no-VIT, 50%-VIT, and 100%-VIT cases produce higher surface temperatures as insulation is added along the production leg. Across all modeled flow rates (50–250 kg/s), the highest return temperatures occur at 100–150 kg/s, while the benefit declines at 200–250 kg/s because reduced residence time limits additional heat uptake.

Across all flow rates, the no-VIT case shows the largest temperature decline along the wellbore, while both 50% and 100% VIT maintain much higher temperatures throughout the vertical section. The improvement from adding insulation is far more pronounced when going from 0% to 50% VIT than from 50% to 100%. At the highest flow rate of 250 kg/s, the 50% VIT case exceeds the 100% VIT case, indicating limited additional benefit from full coverage at high mass flow rates.

4.2 Thermal and Electrical Output: How Insulation and Fluid Choice Interact

Figures 10–12 and 13–14 show that insulation coverage and fluid choice strongly affect electrical power output across flow rates. At low flows (50–100 kg/s), water produces more power in all VIT cases because it returns hotter to surface and does not experience Joule-Thomson cooling. At higher flows (150–250 kg/s) sCO_2 ultimately delivers the highest electrical output at elevated flow rates, regardless of insulation length.

4.3 Water vs. sCO_2 Surface Temperatures at 50% VIT

Figures 15 and 16 compare the produced temperature profiles for water and sCO_2 at 250 kg/s and 150 kg/s under 50% VIT. The results show that at 150 kg/s, water reaches a higher surface temperature than sCO_2, consistent with the expected Joule-Thomson cooling of CO_2 during ascent. However, at the higher flow rate of 250 kg/s, the trend reverses and sCO_2 returns to the surface at a higher temperature than water. The higher flow reduces residence time in the vertical section and limits the magnitude of Joule-Thomson cooling, allowing sCO_2 to preserve more of the heat absorbed in the subsurface.

Figures 17 and 18 show that thermal power increases with flow rate for both fluids, with water having higher thermal power than sCO_2 at all flow rates. When converted to electrical power using the assumed efficiencies (~10% for water ORC and ~23% for sCO_2), water has higher electrical power outputs at flow rates below 150 kg/s. However, above 150 kg/s sCO_2 has higher electrical power output.

4.4 Economic Implications: ROI vs. VIT Coverage and Flow

Table 4 pairs electrical power output with ROI (years) for 50% and 100% VIT at 50–250 kg/s. Two patterns stand out:

50% VIT shows improving ROI with higher flow: from 3.3 years at 50 kg/s down to 1.5 years at 250 kg/s, enabled by substantial electrical output growth (2.3 → 11.53 MWe).

100% VIT shows worsening ROI with higher flow: increasing from 3.50 years at 50 kg/s to 3.7 years at 250 kg/s, despite electrical output rising (3.1 → 11.29 MWe). The interpretation is that full insulation's added cost outpaces the incremental electrical benefit at high flow rates. In other words, diminishing returns from going to 100% VIT become more pronounced as mass flow increases.

5 CONCLUSION

Across all analyses, 50% VIT consistently delivers the strongest overall performance, capturing most of the thermal benefit of full insulation while avoiding the diminishing returns observed at higher flow rates. Water produces more electrical power at lower flow rates because it returns higher surface temperatures and does not experience Joule-Thomson cooling, while sCO_2 overtakes water at higher flows due to its higher conversion efficiency and reduced Joule-Thomson ooling at elevated mass flow. Economically, the advantage of 50% VIT increases with flow rate, whereas 100% VIT becomes less cost-effective as its added expense outweighs its modest performance gains. Overall results show that deploying 50% VIT (13 3/8-inch OD with 9 5/8-inch ID) at 250 kg/s and a bottom-hole temperature of 217.7 °C increases electrical output by roughly 1.35 MWe over the 10.18 MWe baseline without insulation, assuming a representative 23% thermal-to-electric efficiency. This configuration yields an ROI of 1.53 years, demonstrating that partial insulation provides the optimal balance of thermal performance, power generation, and economic return.

While the present analysis provides valuable insights into the influence of working fluid, flow rate, and insulation configuration, several opportunities remain to extend and refine the study. Future work should incorporate a more detailed sensitivity analysis on key assumptions such as injection temperature, wellhead pressure, reservoir permeability, convective heat flow, and thermal conductivity of cement and casing.

6 REFERENCES

Abid, K., Romero Tellez, M.L., and Teodoriu, C.: Long Term Thermal Conductivity of Neat Cement (C, G, H) for Geothermal Applications and Its Impact on Geothermal Well Behavior, Proceedings, 49th Workshop on Geothermal Reservoir Engineering, Stanford University, Stanford, California, USA (2024).

Enverus (2025): Enverus: *Online Well Log and Subsurface Temperature Database*, accessed 2024. Available at: https://www.enverus.com/

FavPNG: Critical Point Supercritical Fluid Supercritical Carbon Dioxide Phase Diagram [PNG Image], (n.d.).

National Energy Technology Laboratory (NETL): NETL Supported Lower Cost Supercritical Carbon Dioxide Turbine Technology Successfully Demonstrated, (2024).

Nielson, J., Simpkins, D., and Katcher, K.: Technoeconomic Analysis of a Geothermal sCO_2 Thermosiphon Power Plant (Paper No. 189), Proceedings, 7th International Supercritical CO_2 Power Cycles Symposium, San Antonio, Texas, USA (2022).

Power Magazine: Breakthrough for sCO_2 Power Cycle as STEP Demo Completes Phase 1 of 10 MW Project, POWER Magazine (2024).

Tison, R.: Researchers Find West Texas Region Holds Promise for Geothermal Production, Texas Geothermal Energy Alliance (TXGEA), May 17, 2024.

U.S. Department of Energy: sCO_2 Power Cycles, Office of Energy Efficiency & Renewable Energy, (2024).

USGS (2025): U.S. Geological Survey (USGS): *National Geothermal Data System (NGDS): Temperature Gradient and Bottom-Hole Temperature Dataset*, accessed 2024. Available at: https://data.usgs.gov/

Wang, S., Jian, L., Shu, Z., Chen, S., and Chen, L.: *A High Thermal Conductivity Cement for Geothermal Exploitation Application*, Natural Resources Research, 29, 3675–3687 (2020).

White, M.: Numerical Investigation of CLG Systems in Deep Geothermal Reservoirs, Geothermics, 116, (2024).

White, M., Vasyliv, Y., Beckers, K., Martinez, M., Balestra, P., Parisi, C., Augustine, C., Bran Anleu, G., Horne, R., Pauley, L., Bettin, G., Marshall, T., and Bernat, A.: Numerical Investigation of CLG Systems in Deep Geothermal Reservoirs, Proceedings, World Geothermal Congress, (2024).

Wisian, K., Ross, M., Bhattacharya, S., Khaled, M., Young, B., Chapman, D., and Turan, A.: Presidio County Geothermal Assessment, Bureau of Economic Geology, The University of Texas at Austin, 88 pp., May 2024.

Vasyliv, Y.V., Bran Anleu, G.A., Kucala, A.K., Subia, S.R., and Martinez, M.J.: Analysis and Optimization of a Closed Loop Geothermal System in Hot Rock Reservoirs, GRC Transactions, 45, (2021).

Zhang, F., and Li, L.: Study on Thermal Conductivity of Thermal Insulation Cement in Geothermal Well, Frontiers in Earth Science, 10, (2022).

Zhou, W., Wang, C., Meng, R., Chen, Z., Lu, H., and Chi, J.: Study on Thermal Insulation Cement and Its Thermal Insulation Characteristics for Geothermal Wells, Scientific Reports, 13, (2023).